

Numerical Simulation of Particle Dispersion in a Spatially Developing Mixing Layer*

Zhiwei Hu

AFM Research Group, School of Engineering Sciences,
University of Southampton, Southampton SO17 1BJ, England
z.hu@soton.ac.uk

Xiaoyu Luo

Department of Mechanical Engineering,
University of Sheffield, Sheffield S1 3JD, England
x.y.luo@sheffield.ac.uk

Kai H. Luo

Department of Engineering, Queen Mary & Westfield College,
University of London, London E1 4NS, England
k.h.luo@qmw.ac.uk

Communicated by T. B. Gatski

Received 7 June 2001 and accepted 19 February 2002

Abstract. Although there have been several numerical studies on particle dispersion in mixing layers, most of them have been conducted for temporally evolving mixing layers. In this study, numerical simulations of a spatially developing mixing layer are performed to investigate particle dispersion under various conditions. The full compressible Navier–Stokes equations are solved with a high-order compact finite difference scheme, along with high-order time-integration. Accurate non-reflecting boundary conditions for the fluid flow are used, and several methods for introducing particles into the computational domain are tested. The particles are traced using a Lagrangian approach assuming one-way coupling between the continuous and the dispersed phases. The study focuses on the roles of the large-scale vortex structures in particle dispersion at low, medium and high Stokes numbers, which highlights the important effects of interacting vortex structures in nearby regions in the spatially developing mixing layer. The effects of particles with randomly distributed sizes (or Stokes numbers) are also investigated. Both instantaneous flow fields and statistical quantities are analyzed, which reveals essential features of particle dispersion in spatially developing free shear flows, which are different from those observed in temporally developing flows. The inclusion of the gravity not only modifies the overall dispersion patterns, but also enhances stream-crossing by particles.

1. Introduction

Understanding the mechanisms of particle movement in free shear flows is very important for many industrial, environmental and biomedical applications. Examples include: dispersion of diesel and jet engines

* This work was supported by the EPSRC under Grant No. GR/L58699.

emissions in the atmosphere; medicines dispersed by blood through the vessels; and dust inhaled into human lungs. All of these problems are related to solid particle dispersion in fluid flows, which often involves complicated interactions between the dispersed (solid) phase and the continuous (fluid) phase. Depending on the volume fraction of the dispersed phase, there can be one-way, two-way or four-way coupling. For diluted systems (volume fraction $< 10^{-6}$), only the flow effects on particles are important. For medium particle concentrations (volume fraction $> 10^{-6}$), particles will affect the flow field too. For dense particle systems (volume fraction $> 10^{-3}$), particle–particle interactions become significant. Even in the simplest case of one-way coupling, our current understanding is very limited, since different scales of flow motions (e.g. large scales versus small scales) have different effects on particle transport. If the effects of different particle sizes, shapes and physical properties are included, the full problem becomes prohibitively complex. Needless to say, studies in the area inevitably involve considerable simplifications. Free mixing layers have been extensively used as a prototype flow for fundamental studies over the past few decades. Since the early work of Snyder and Lumley (1971) on the turbulent mixing layer, many experiments have been conducted (e.g. Weisbrot and Wygnanski, 1988; Wygnanski and Weisbrot, 1988) to study the coherent structures and especially the pairing processes of plane mixing layers. Direct Numerical Simulation (DNS) is a relatively new tool but has been successfully used for both temporal (Rogers and Moser, 1992; Moser and Rogers, 1993; Vreman *et al.*, 1996) and spatial mixing layers (Stanley and Sarkar, 1997). A comprehensive review on DNS of single-phase flow and turbulence can be found in Moin and Mahesh (1998).

More recently, DNS on particle dispersion in temporal mixing layers and isotropic turbulence have also been published. Ling *et al.* (1998) simulated the particle dispersion in a three-dimensional temporal mixing layer and obtained the dispersion patterns for particles of different Stokes numbers. Elghobashi and Truesdell (1992, 1993) and Truesdell and Elghobashi (1994) simulated particle dispersion in a decaying isotropic turbulence, and considered the two-way coupling between the particles and the fluid flow, which included the effects of gravity. Wang and Maxey (1993) calculated the particle motion in a stationary homogeneous isotropic turbulence. They found that the average settling velocity is increased significantly for particles with inertial response time and for still-fluid settling velocity comparable with the Kolmogorov scale of turbulence. Marcu *et al.* (1996) and Marcu and Meiburg (1996) investigated the effects of braid vortices on the dispersion of particles, and observed that only very low Stokes number particles accumulate at the vortex center. For moderate values of Stokes numbers, the particles remain trapped on closed trajectories around the vortex centers, which can be opened by further increasing the Stokes number. Using the database from particle-laden isotropic turbulent flow simulations, Squires and Eaton (1994) analyzed the influence of particles on turbulence and found that the balance between entropy production by turbulent vortex stretching and destruction is disrupted by momentum exchange with the particle cloud.

These studies demonstrated that DNS is capable of revealing detailed mechanisms behind movement, due to its ability of resolving the whole range of time and length scales. Simulations have been carried out in idealized isotropic turbulence or temporally developing mixing layers, which are quantitatively and in some aspects qualitatively different from the more realistic spatially developing shear-layer flows. The latter have not been sufficiently investigated, partly because of the higher computational cost but more importantly because of increased complexity in the numerical treatment. For example, how to treat the particles entering and leaving the finite computational domain is still an open question. Furthermore, almost all of the previous simulations involving particles used incompressible flow formulations. That is understandable, given the fact that most practical problems occur in a low-speed environment. However, the dispersion of emissions from jet engines and the whipping-up of dusts in hurricanes are clearly examples of particle movement in a high-speed flow environment. Therefore, a compressible flow formulation is also important.

This paper focuses on particle dispersion in spatially developing free shear flows. A formulation based on the complete unsteady compressible Navier–Stokes equations is employed. The numerical discretization, solution and specification of boundary conditions all feature high-order methods, which are accurate and memory-saving. A Lagrangian approach is used to trace the particles, which are passively transported by the fluid flow. The investigation focuses on the effects of spatially developing vortex structures on particle dispersion in a transitional free shear flow. A detailed parametric study is conducted on the effects of the Stokes number and the gravity. This study marks only the first stage in a comprehensive study aimed at understanding and predicting flow-particle interactions in a three-dimensional compressible turbulent medium.

The organization of the paper is as follows: Section 2 presents the basic governing equations for compressible flow and particle motion. Section 3 describes the numerical treatment of particle-laden flow

simulations. The simulation results are presented in Section 4, with detailed analysis. Finally, conclusions are drawn in Section 5, together with discussions on the limitations of the present study and possible future work.

2. Governing Equations

2.1. The Governing Equations for the Continuous Phase

The non-dimensional governing equations for compressible flow are:

$$\frac{\partial \rho}{\partial t} = -\frac{\partial(\rho u_j)}{\partial x_j}, \quad (1)$$

$$\frac{\partial(\rho u_i)}{\partial t} = -\frac{\partial(\rho u_i u_j)}{\partial x_j} - \frac{\partial p}{\partial x_i} + \frac{\partial \tau_{ij}}{\partial x_j}, \quad (2)$$

$$\frac{\partial E_T}{\partial t} = -\frac{\partial[(E_T + p)u_j]}{\partial x_j} - \frac{\partial q_j}{\partial x_j} + \frac{\partial(u_i \tau_{ij})}{\partial x_j}. \quad (3)$$

For the present mixing layer, all variables are non-dimensionalized by the upper free stream quantities (density ρ_1^* , velocity U_1^* and temperature T_1^*) and the initial vorticity thickness of the mixing layer $\delta_\omega = (U_1^* - U_2^*)/|du_0^*/dy^*|_{\max}$. U_2^* is the lower free stream velocities, $U_2^* < U_1^*$, u_0^* is the initial velocity. $E_T = \rho(e + \frac{1}{2}u_i u_i)$ is the non-dimensional total energy, e is the internal energy determined by $e = c_v T$ where c_v is the constant volume specific heat. The non-dimensional shear stress tensor τ_{ij} is related to the shear rate by the Newtonian constitutive equation:

$$\tau_{ij} = \frac{\mu}{Re} \left(\frac{\partial u_i}{\partial x_j} + \frac{\partial u_j}{\partial x_i} - \frac{2}{3} \frac{\partial u_k}{\partial x_k} \delta_{ij} \right), \quad (4)$$

and q_j is determined by the Fourier heat conduction law:

$$q_j = -\frac{\mu}{(\gamma - 1)M_1^2 Pr Re} \frac{\partial T}{\partial x_j}. \quad (5)$$

Here $M_1 = U_1^*/C_1^*$ is the upper free stream Mach number, C_1^* is the upper free stream sound speed and $C_1^* = \sqrt{\gamma R T_1^*}$. The Reynolds number of the flow is defined as $Re = \rho_1^* U_1^* \delta_\omega / \mu_1^*$, and the Prandtl number as $Pr = c_p \mu^* / k^*$, where k^* is the thermal conductivity, and c_p is the constant pressure specific heat. The non-dimensional viscosity of fluid is assumed to follow a power law $\mu = T^{0.76}$, where the exponent is chosen according to White (1974).

The perfect gas law is then

$$p = \frac{\rho T}{\gamma M_1^2} = \rho(\gamma - 1)e. \quad (6)$$

The transport equation of a passive scalar f is also solved for flow visualization (Ramaprian *et al.*, 1989):

$$\frac{\partial(\rho f)}{\partial t} = -\frac{\partial(\rho f u_j)}{\partial x_j} + \frac{1}{S_C} \frac{\partial}{\partial x_j} \left(\frac{\mu}{Re} \frac{\partial f}{\partial x_j} \right). \quad (7)$$

The Schmidt number $S_C = \mu^* / \rho^* D^*$ (D^* is the diffusion coefficient) is assumed to be constant.

In the present study we take both the Prandtl number and the Schmidt number to be unity.

2.2. The Governing Equation for the Dispersed Phase

Using the equation of motion for a small rigid sphere in a non-uniform flow derived by Maxey and Riley (1983), and non-dimensionalizing the equation in the same way as for the continuous phase, we obtain

$$\begin{aligned}
 \frac{d\mathbf{v}}{dt} = & \underbrace{\frac{1}{St} \left(\mathbf{u} - \mathbf{v} + \frac{d_p^2}{24} \nabla^2 \mathbf{u} \right)}_1 + \underbrace{(1 - \alpha) \frac{1}{St} \frac{\tau_p}{U_1} \mathbf{g}}_2 \\
 & + \underbrace{\alpha \frac{D\mathbf{u}}{Dt}}_3 - \underbrace{\frac{1}{2} \alpha \frac{d}{dt} \left(\mathbf{v} - \mathbf{u} - \frac{1}{40} \frac{d_p^2}{\delta_\omega} \nabla^2 \mathbf{u} \right)}_4 \\
 & - \underbrace{\frac{9\alpha\delta_\omega}{d_p\sqrt{\pi Re}} \int_0^t \frac{(d/d\tau) \left[\mathbf{v} - \mathbf{u} - \left(\frac{d_p^2}{24\delta_\omega^2} \nabla^2 \mathbf{u} \right) \right]}{(t - \tau)^{1/2}} d\tau}_5, \tag{8}
 \end{aligned}$$

where \mathbf{v} is the non-dimensional velocity of particle; \mathbf{u} is the non-dimensional velocity of the undisturbed fluid evaluated at the center of the particle; d_p is the non-dimensional particle diameter, $d_p = d_p^*/\delta_\omega^*$; α is the ratio of the density of fluid ρ^* to the density of particles ρ_p^* , $\alpha = \rho^*/\rho_p^*$; d/dt denotes a Lagrangian time derivative following the particle, and D/Dt denotes a time derivative using the undisturbed fluid velocity as the convective velocity. St is the Stokes number of the particle, which is defined as the ratio of the particle momentum response time τ_p to the flow field time scale:

$$St = \frac{\tau_p}{\delta_\omega/U_1} = \frac{\rho_p d_p^2 / 18\mu}{\delta_\omega/U_1}. \tag{9}$$

The terms on the right-hand side of (8) are the force of Stokes viscous drag, the gravity, the effect of pressure gradient of the undisturbed flow, the added mass and augmented viscous drag from the Basset history term (the Basset force), respectively.

In the present study a diluted system is considered, with the following assumptions:

- (1) the particles are rigid spheres with identical diameter d_p and density ρ_p ,
- (2) the density of a particle is much larger than the density of the fluid, and
- (3) the effect of particles on the fluid is negligible.

With these assumptions, the effect of pressure gradient, added mass and the Basset force in (8) are also negligible (Ling *et al.* 1998). Hence the non-dimensional Lagrangian particle equation becomes

$$\frac{d\mathbf{v}}{dt} = \frac{f_p(\mathbf{u} - \mathbf{v})}{St} + (1 - \alpha) \frac{1}{St} \frac{\tau_p}{U_1} \mathbf{g}, \tag{10}$$

where f_p is the modification factor for the Stokes drag coefficient. As long as the particle Reynolds number, $Re_p = |\mathbf{u} - \mathbf{v}|d_p/\nu$, is less than 1000, f_p can be represented reasonably by $f = 1 + 0.15 Re_p^{0.687}$ (Ling *et al.* 1998).

The particle position can be obtained by integrating the following equation:

$$\frac{d\mathbf{x}}{dt} = \mathbf{v}. \tag{11}$$

3. Simulation Details

The computational domain is chosen to be a rectangular box with a size of $L_x \times L_y = 250 \times 30$, as shown in Figure 1. The grid points used are $N_x \times N_y = 501 \times 61$, which are uniformly distributed in the x direction, and stretched in the y direction by

$$y(j) = \frac{1}{2} \frac{\sinh(\beta_y s(j))}{\sinh(\beta_y)} L_y, \quad (12)$$

where $s(j) = -1 + 2j/(N_y - 1)$, and β_y is the stretching factor, chosen to be $\beta = 1.3$ for all the simulations. The grid points were chosen with reference to other published simulations as well as our resolution tests.

The convection velocity of a mixing layer is defined as $U_c^* = (U_1^* + U_2^*)/2$, and the convective Mach number as $M_c = (U_1^* - U_2^*)/(C_1 + C_2)$, where C_1 and C_2 are the sound speeds of the upper and lower free streams, respectively. We choose $M_c = 0.04$, Reynolds number $Re = 200$ and $\lambda = (U_1^* - U_2^*)/(U_1^* + U_2^*) = 0.25$.

3.1. Initial Conditions

The initial velocity profile of the flow field is set to be a hyperbolic tangent profile

$$u_0^*(y) = \frac{U_1^* + U_2^*}{2} + \frac{U_1^* - U_2^*}{2} \tanh\left(\frac{2y^*}{\delta_\omega^*}\right). \quad (13)$$

The initial mean-temperature profile is specified by a Crocco–Busemann relation:

$$T_0 = 1 + M_1^2 \frac{\gamma - 1}{2} (1 - u_0^2), \quad (14)$$

where $M_1 = 0.05$. The mean pressure is assumed to be uniform.

The inflow perturbation has strong influence on the growth of the mixing layer. Suitably selected initial perturbations can enhance the growth of the mixing layer (Ho and Huerre, 1984; Inoue, 1995). Three types of inflow perturbations have been tested:

Perturbation 1: $u' = A_0 \sin(2\pi f_0 t)$,

Perturbation 2: $u' = A_0 \sin(2\pi f_0 t) + A_1 \sin(2\pi f_1 t + \beta_1)$, and

Perturbation 3: $u' = A_0 \sin(2\pi f_0 t) + A_1 \sin(2\pi f_1 t + \varphi_1)$,

where f_0 is the most unstable frequency from the linear stability analysis, f_1 is the first subharmonic frequency and β_1, φ_1 are the phase shifts between the two frequencies. In perturbation 2 the phase shift β_1 is a constant, chosen to be 45° , whereas in perturbation 3 a random walking phase shift $\varphi_1 (< 15^\circ)$ is introduced (Sandham and Reynolds, 1989). These perturbations are used to induce vortex pairing in the mixing layer.

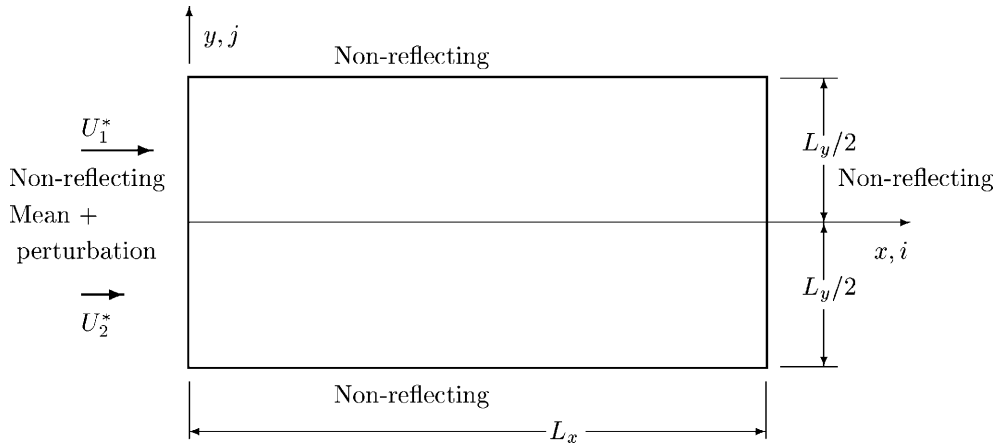


Figure 1. Computational domain and boundary conditions.

3.2. Boundary Conditions

One of the greatest difficulties in simulating spatially developing shear flow is the formulation of the boundary conditions required for the open computational domain, especially for compressible viscous flow. Since in most cases the computational box is finite, information passing through the boundaries from outside acts as a source of errors, which could quickly contaminate the numerical solution inside. As a countermeasure, a number of non-reflecting numerical boundary conditions (e.g. Thompson, 1987; Poinso and Lele, 1992) have been devised in recent years, with considerable success. Thompson (1987) developed a non-reflecting boundary condition scheme based on the Euler equations. The basic idea is to allow flow structures in the interior of the computational domain to pass through the boundary while keeping the spurious waves generated at the boundary out. Poinso and Lele (1992) generalized Thompson's formulation by starting from the Navier–Stokes equations with the viscous terms. In this study the non-reflecting boundary conditions of Poinso and Lele (1992) are applied to all the boundaries, as shown in Figure 1. Results from the following simulations show that the boundary conditions worked very well in keeping spurious waves out of the computational domain.

3.3. Particle Treatment

At the beginning of each simulation, particles are uniformly placed at each grid point and set in equilibrium with the fluid. As the mixing layer develops, they are transported by the fluid and some of them may move out of the computation domain. To keep constant number of particles inside the box, new particles need to be added in. There are several different ways of adding particles. Three possibilities are listed below:

- (1) Keep a constant number of particles in the domain. Every particle moving out of the domain is re-entered from the inlet boundary at the same y , but is set to an equilibrium status with the local fluid.
- (2) Add equal numbers of particles in both upper and lower streams at the same time interval, $\Delta t = \Delta x/U_c$.
- (3) Keep the same particle density in both undisturbed streams. This means adding particles into the upper and lower streams at different time intervals, $\Delta t_1 = \Delta x/U_1$ and $\Delta t_2 = \Delta x/U_2$.

The first method is very similar to the method used in the temporal mixing layer, which is not very suitable for the spatial mixing layer as the latter has different boundary conditions at the inflow and the outflow. The second method tends to leave too few particles in the upper stream before the mixing layer is properly evolved. This is because particles in the upper stream move out of the domain faster. The third method gives a uniform particle distribution in the undisturbed streams all the time. This is more likely to happen in a realistic spatially developing mixing layer. The three options were extensively tested and the third method was found to be more suitable and thus adopted in the final simulations.

3.4. Numerical Methods

The governing equations are spatially discretized using the compact finite difference schemes developed by Lele (1992). This gives a sixth-order accuracy for all the inner grid points and a third-order accuracy for the boundary points. The discretized governing equations for both the continuous and the dispersed phases are marched in time with an explicit third-order compact-storage Runge–Kutta method. The time step is set according to a *CFL*-number criterion, which includes effects of both convection and viscous diffusion, as follows:

$$\Delta t = \frac{CFL}{D_c + D_d}, \quad (15)$$

where

$$D_c = \pi c \left(\frac{1}{\Delta x} + \frac{1}{\Delta y} + \frac{1}{\Delta z} \right) + \pi \left(\frac{|u_x|}{\Delta x} + \frac{|u_y|}{\Delta y} + \frac{|u_z|}{\Delta z} \right),$$

$$D_d = \frac{\pi^2 \mu}{(\gamma - 1) \rho M_1^2 Re Pr} \left[\frac{1}{(\Delta x)^2} + \frac{1}{(\Delta y)^2} + \frac{1}{(\Delta z)^2} \right],$$

where c is the local sound speed. The theoretical value for CFL is $\sqrt{3}$ for stability of the above time advancement scheme. In actual simulations, preliminary numerical tests were conducted to choose the value for CFL for a particular problem. Once CFL was determined, the time step was computed for each cell and the smallest value was used for time advancement. At each sub-time-step of the Runge–Kutta method, after solving the fluid equations, the flow velocities are interpolated at third-order accuracy to each particle's position.

4. Results

4.1. The Effects of Perturbations on the Mixing Layer

The passive scalar contours of the mixing layer with the three different initial perturbations are shown in Figure 2. The two two-frequency perturbations give much enhanced mixing layer growth rates by triggering the vortex pairing processes. This is confirmed by the corresponding momentum thickness spread shown in Figure 3. The single-frequency perturbation saturates much faster, resulting in a rapid drop in the momentum thickness at about $x = 200$. On the other hand, the two-frequency perturbations produce almost monotonic increase in the momentum thickness, with perturbation 3 showing the most consistent trend. Hence perturbation 3 is used to calculate all the following results.

4.2. Particle Dispersion with Different Stokes Numbers

Dispersion of particles with St in the range of $0.1 - 100$ is calculated for zero gravity first ($g = 0$). Figure 4 shows the dispersion pattern of particles with $St = 4$ at $t = 315$. In the upstream part of the spatial mixing layer ($x = 0 - 90$), the distribution of particles is scarcely affected by the fluid flow, due to a lack of large organized structures. As the first few large vortices appear due to the Kelvin–Helmholtz instability, particles are transported across the free streams, resulting in non-uniform particle dispersion patterns. Particles are seen to be moving away from the vortex cores while accumulating in the regions surrounding the vortices and in the braid regions. After the vortex merging process following the vortex pairing, larger vortices are

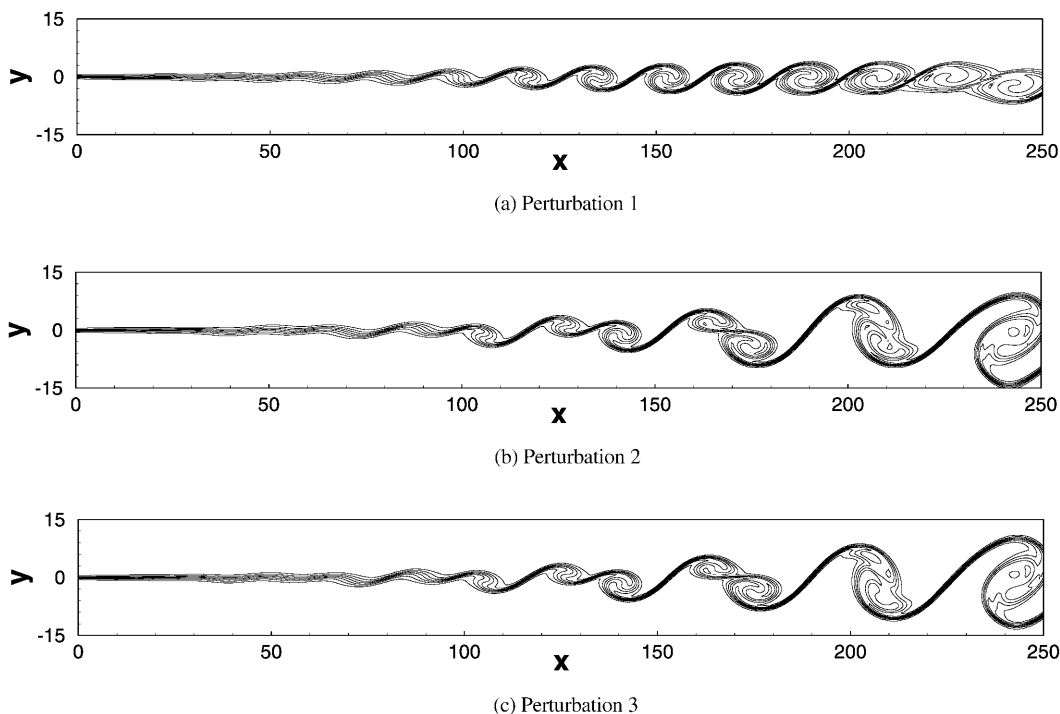


Figure 2. Passive scalar contours of the mixing layer with different perturbations at $t = 315$.

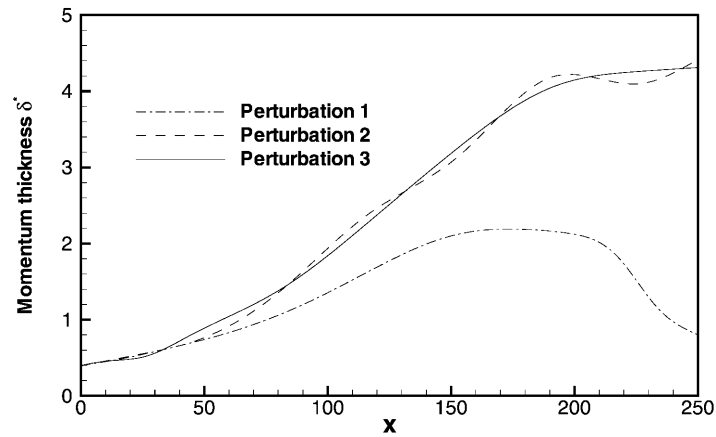


Figure 3. Momentum thickness of the mixing layer under different perturbations.

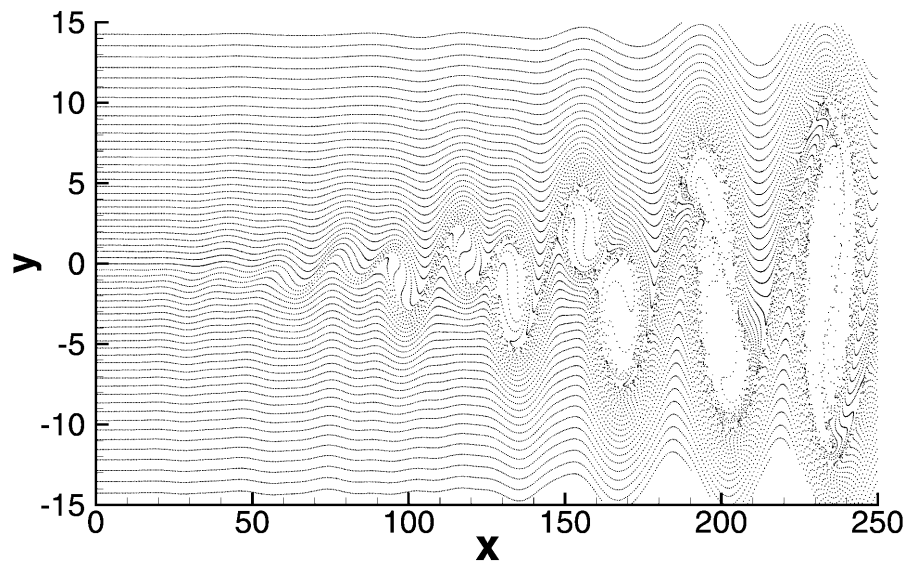


Figure 4. Particle dispersion pattern in the spatially developing mixing layer at $t = 315$ for $St = 4$. Plotted are the particle positions.

created, which draw particles from larger distances into the high shear layer regions. Particle distribution becomes even more non-uniform, with a large area (the vortex core) depleted of particles.

The particle movement and their distribution in the mixing layer are strongly influenced by the size and consequently the response time of particles, which is measured by the Stokes number. The detailed particle dispersion patterns resulting from different Stokes numbers are shown in Figure 5 for $x = 100 - 250$. The corresponding vortex contours of the flow field are shown in Figure 5(a). It is seen that particles of small Stokes numbers ($St = 0.1, 1$) are carried by the fluid all around the flow field, including the vortex cores. Since these particles respond quickly to the change of fluid motions, they can follow the fluid closely, which lead to particle dispersion patterns closely resembling the fluid vortex structures. In other words, particles with very small Stokes numbers are in a quasi-equilibrium status with the fluid. In contrast, particles with moderate Stokes numbers (i.e. $St = 4, 10$) tend to accumulate around the circumference of a vortex and along the braid between two vortices, which results in some “blank” regions in which few solid particles are found. This is because of the effects of flow field strains combined with the centrifugal effects. For the high Stokes number case ($St = 100$), the general dispersion pattern is similar to that of the medium Stokes number cases. However, since the particles are so slow to respond and follow the fluid motion, even the roll-up and rotation of large vortex structures do not disturb many of the particles. Consequently, particle accumulation in the braid regions and around the vortices is less effective. Some particles even cross the vortex core regions

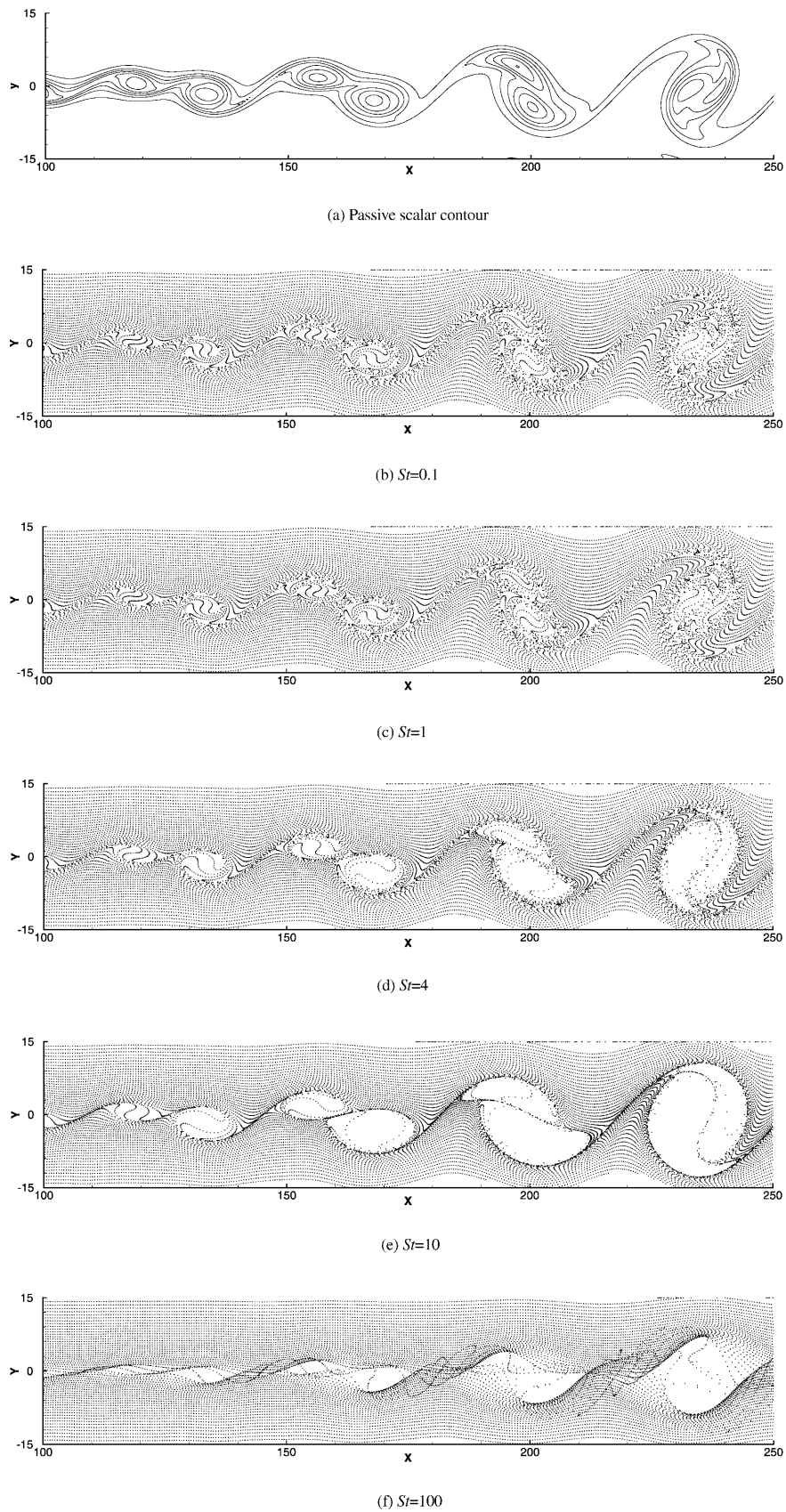


Figure 5. The passive scalar contour and the particle dispersion patterns for different Stokes numbers for $x = 100 - 250$ at $t = 315$.

due to their large inertia. As a result, the depleted regions (without particles) are much smaller than the sizes of the vortices and particles in the far field are not affected much.

These observations are broadly in agreement with previous results from temporal mixing layers (e.g. Martin and Meiburg, 1994), with some exceptions. For example, the dispersion pattern at $St = 1$ in the temporal mixing layer of Martin and Meiburg (1994) is very different from that observed in the present study. In their simulation, particles do not fill the vortex cores, contrary to the finding from Figure 5(c). Instead, their result at $St = 1$ looks like the present results at higher Stokes numbers, e.g. in Figure 5(d). Their result is surprising in a physical sense because a unity Stokes number suggests that the time scale of the fluid flow is equal to that of the particle movement, so that particles should follow the vortex motion closely. Their result to the contrary suggests that the use of the temporal mixing layer model might have changed the physics of the particle dispersion. This topic is revisited in the next section.

The most interesting feature of the present spatial mixing layer, however, is the presence of interactions between nearby vortex structures, which affect particle transport. As a result, the dispersion pattern of particles is not symmetric, in contrast to the findings in temporal mixing layers (Ling *et al.*, 1998). This difference can be explained in the following. In the case of temporal mixing layers, particles which go out of the computational domain are re-entered from the inflow, so these particles are always under the influence of the same vortex. For a spatial mixing layer, however, particles which are transported from one vortex into another usually have different structures. In the present mixing layer, the differences in vortices at different streamwise locations are quite large, due to vortex pairing. In addition, it is noted that the upper free stream velocity is greater than the convection velocity of mixing layer U_c (the rate of convection of the large vortices), and the lower stream velocity is smaller than U_c . Thus particles in the upper free stream move faster than the vortex, and slower in the lower stream. Hence, particles in the upper stream tend to catch up with the vortex in front and be transported by the next vortex. However, particles in the lower stream are left behind the vortex in front and are affected by the vortex from behind. The net result is that more particles from the upper stream are transported to the lower stream than from the lower to the upper stream. This point is revisited in Section 4.5. These special features of particle dispersion in the spatial mixing layer are absent from temporal simulations.

The root mean square of the particle number per cell for each x station, $N_{rms}(x)$ (Ling *et al.* 1998), is used to quantify the distribution of particles along the streamwise direction. $N_{rms}(x)$ is obtained from

$$N_{rms}(x) = \left(\sum_{i=1}^{N_{cp}} \frac{N_i(x)^2}{N_{cp}} \right)^{1/2}, \quad (16)$$

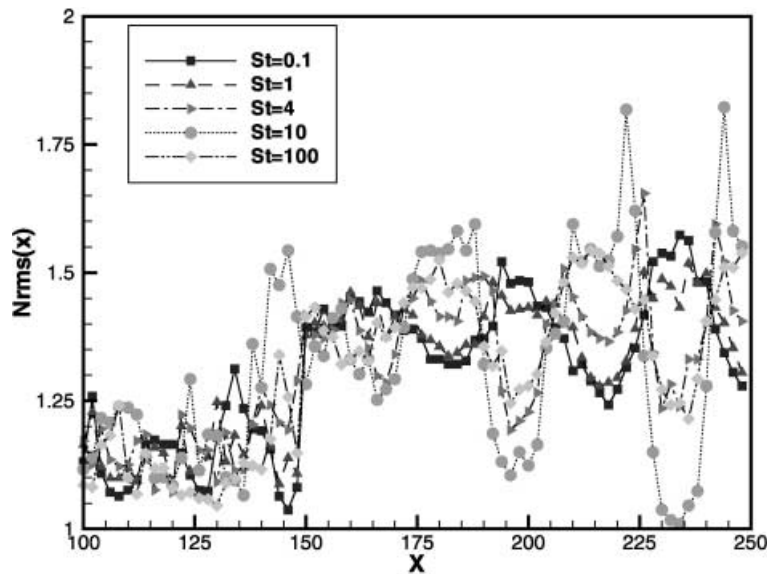


Figure 6. The particle number density $N_{rms}(x)$ for different Stokes numbers.

where N_{cp} is the total number of computational cells in one x station and $N_i(x)$ is the number of particles in the i th cell of that x station. To eliminate the oscillations in N_{rms} due to the use of the limited particle sample in each column, the cell for calculating N_{rms} is chosen to include four streamwise grid points. The concentration of particles with different Stokes numbers along the streamwise direction is shown in Figure 6. The most prominent feature is that the particle concentration is not uniform along the streamwise direction, with alternating high and low concentration regions. The variation (the amplitude of the fluctuations) in the concentration increases in the streamwise direction, reflecting the increasing effects of larger vortices. The Stokes number effects are obvious, with a small Stokes number group ($St = 0.1, 1$) and a high Stokes number group ($St = 4, 10, 100$). For the latter, the low particle concentration regions correspond to the vortex cores while the high concentration regions correspond to the braid regions. For the former group, however, the opposite trend is observed. Thus at small Stokes numbers, the vortices seem to be able to draw particles from surrounding areas and keep them within their borders. Another interesting phenomenon is that the variation in the concentration along the streamwise direction in the small Stokes number cases is much smaller than in the high Stokes number cases. This is because particles of smaller sizes can follow the fluid motion more closely so their concentration is more uniform and less influenced by the strains caused by large vortex structures. The largest variation in the streamwise concentration occurs for $St = 4$, a medium Stokes number. This can be understood as follows: particle concentration (negative divergence) in the braid region between two vortices and around the circumference of a vortex is promoted by flow strains, whose effects are more pronounced in the low to medium Stokes number range. Particle divergence from the vortex core is due to the centrifugal effect, which is more effective for medium to high Stokes numbers, that is, heavy particles. Particle concentration variation in the streamwise direction is due to the combined effects of the above two factors. It thus seems logical that a medium Stokes number, such as $St = 4$, has an optimal combination of the two effects, which gives the largest variation in particle concentration in the streamwise direction.

4.3. Dispersion of Particles with Random Stokes Numbers

In each of the above-mentioned simulations the Stokes number is uniform, although different Stokes numbers are used in different simulations. In reality, however, particles entering a practical system are expected to have different sizes with correspondingly different Stokes numbers. The particle sizes in a chosen system are also expected to have a particular statistical distribution, such as Gaussian. The effects of particle size distributions are especially important and complex for spatially developing mixing layers, as different-sized particles at different locations are affected by different vortex motions. Here without reference to a particular system, we study a case in which the particle size or the Stokes number has a random distribution within the limits of $St = 1 - 100$. Results are shown in Figure 7. It can be seen that the dispersion pattern is highly complex, representing the superposition of different effects. However, some trends are still identifiable. Partly because the Stokes numbers used are all above or equal to 1, the circumference and the braid regions have high particle concentrations, in agreement with earlier observations in the medium and high Stokes number cases. The dispersion patterns seem to be the result of the superposition of the patterns obtained at the individual Stokes numbers concerned. However, the situation would be far more complex if the particle-particle interactions were included.

4.4. Particle Transport Across Streams

The mechanisms behind particle transport in the spatially developing mixing layer can be more clearly identified by focusing on particles crossing streams. In Figure 8 the dispersion patterns of particles originating from the upper stream are shown for different Stokes numbers. It is clear that particle movement initially occurs along the interface between the two free streams. Thus particle concentration increases in regions of high strains, especially in the braid regions. As the vortices roll up, particles are carried from the upper stream to the lower stream by the “tongues” of the large vortices. For particles of small Stokes numbers, they respond quickly and follow the streamlines of the flow. They eventually fill the vortex core regions. Larger particles are less responsive and are reluctant to follow the fast-moving vortex tongues. So they do not fill the vortex cores completely. Even if they are carried by the flow to the vortex core,

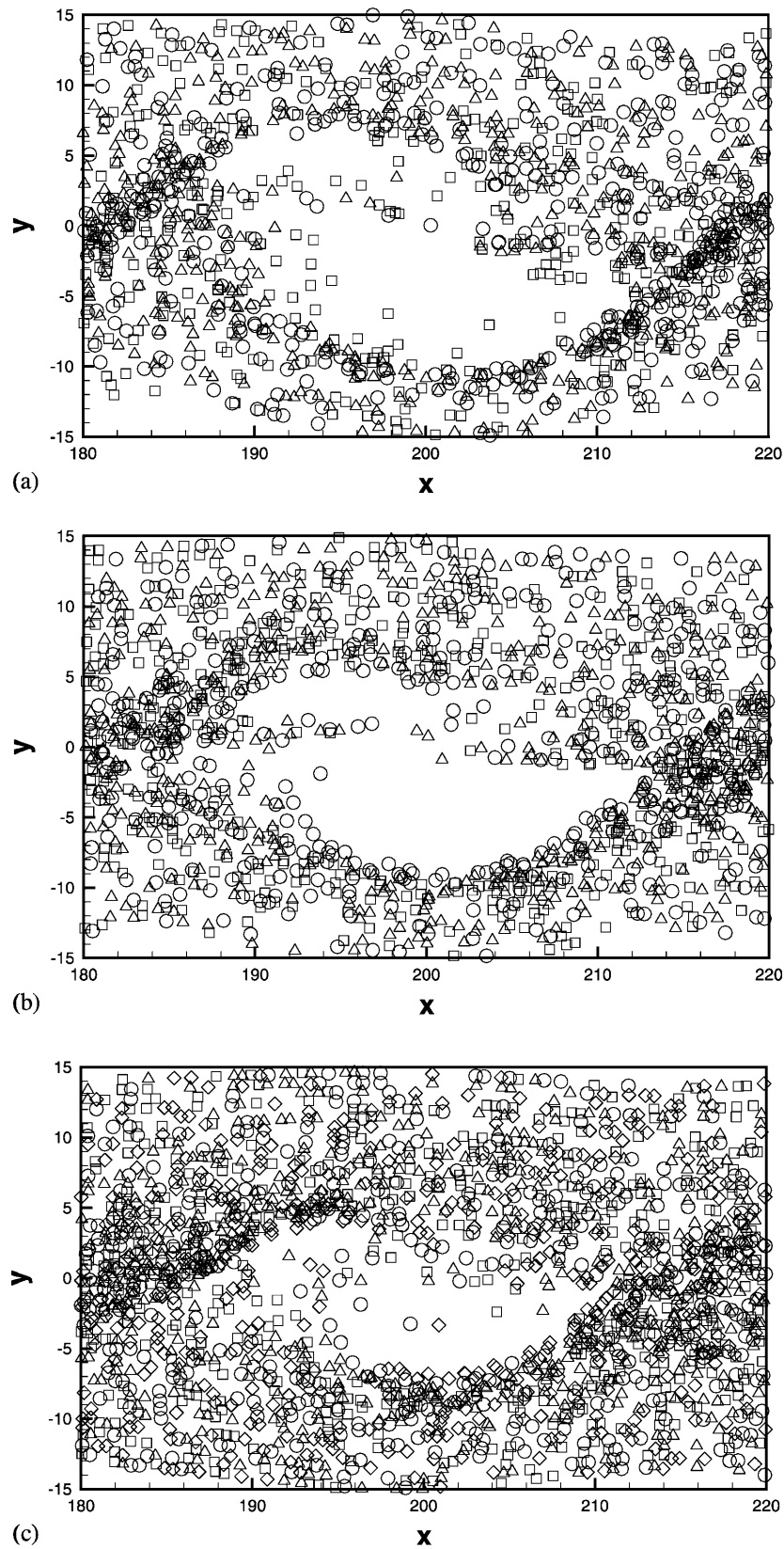


Figure 7. Dispersion pattern resulting from particles of different sizes with randomly distributed Stokes numbers. (a) Square: $St = 1 - 10$; triangle: $St = 10 - 20$; circle: $St = 20 - 30$. (b) Square: $St = 30 - 40$; triangle: $St = 40 - 50$; circle: $St = 50 - 60$. (c) Square: $St = 60 - 70$; triangle: $St = 70 - 80$; circle: $St = 80 - 90$; diamond: $St = 90 - 100$.

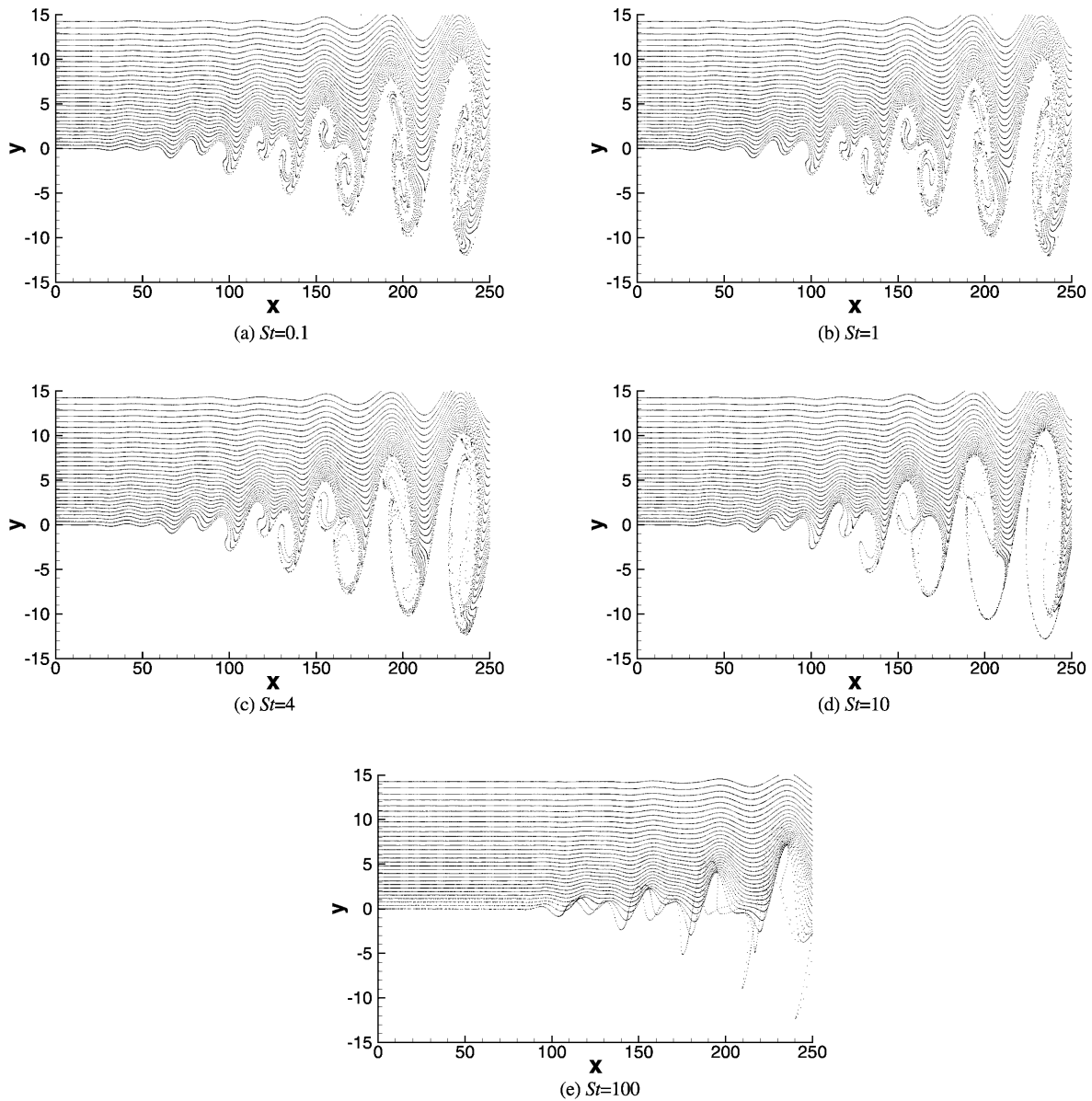


Figure 8. Distributions of particles originating from the upper stream at $t = 315$.

they are drawn away due to the centrifugal effects. This is most noticeable by focusing on the braid region before and after the vortex pairing. Before the vortex pairing, the braid region has high particle concentration. As the vortex pairing process proceeds, the braid region between the pairing vortices gradually becomes the vortex core of the merged vortex. However, due to the centrifugal effect, particles are drawn towards the vortex circumference so that in the end there are very few particles left in the vortex core of the enlarged vortex. In the case of the largest Stokes number ($St = 100$), particles only start to be affected by the flow at about $x = 100$, while in the low Stokes number ($St = 0.1$) case the location is about $x = 50$. In the lateral direction (y direction), the extent to which the large vortices affect the particle movement is also much less. What is interesting in Figure 8(e) is the appearance of particles which oscillate across the stagnation lines along the braid regions. Such particle oscillations have been observed in the stagnation point flow of Martin and Meiburg (1994). These happen because heavy particles of large inertia initially cross the stagnation line, and are then pushed back by flow of the opposite direction. Similar conclusions can be drawn from Figure 9, which shows the corresponding dispersion patterns of particles originating from the lower stream. It is noticed, however, that there is no symmetry or anti-symmetry

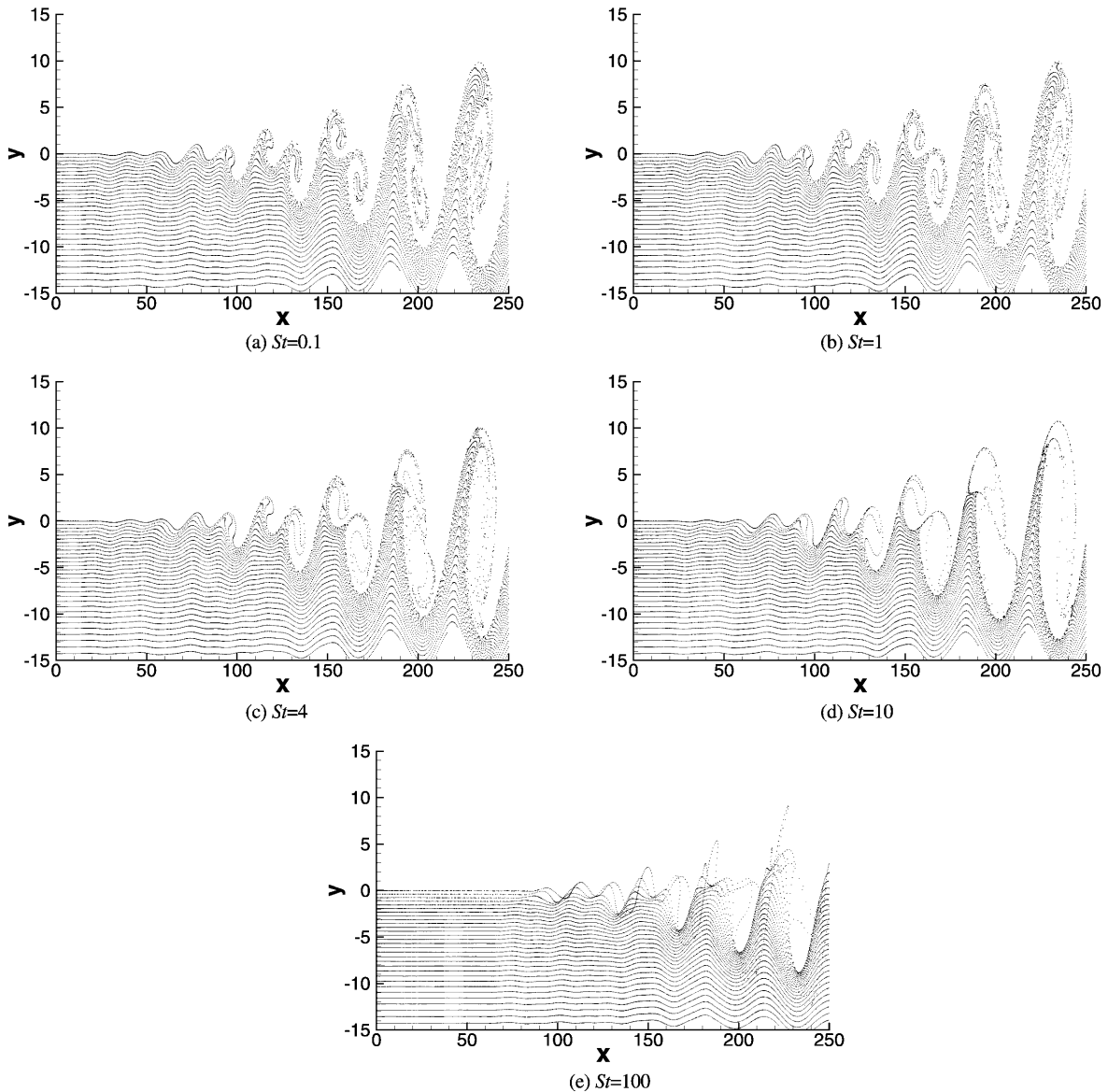


Figure 9. Distributions of particles originating from the lower stream at $t = 315$.

between Figures 8 and 9, due to the vortex interactions in the streamwise direction as discussed above. From these results, the total percentage of particles crossing the streams can be calculated. This is shown in Figure 10 for different Stokes numbers, which confirms the above observations in a quantitative term. It is clear that the percentage of particles transported across streams decreases with the Stokes number, with that percentage three times higher in the low Stokes number ($St = 0.1$) case than in the high Stokes number ($St = 100$) case.

4.5. Influence of Gravity

To investigate the influence of gravity on particle movement, we impose standard gravity, $g^* = 9.81 \text{ m/s}^2$, in the negative y direction. The particle dispersion patterns for $St = 4$ with and without gravity are shown in Figure 11. As expected, particles move downwards in gravity as they are heavier than the fluid. As a result, the dispersion patterns are also changed slightly. Although not plotted, it has been observed that the effects of gravity increase for particles with larger Stokes numbers. The percentage

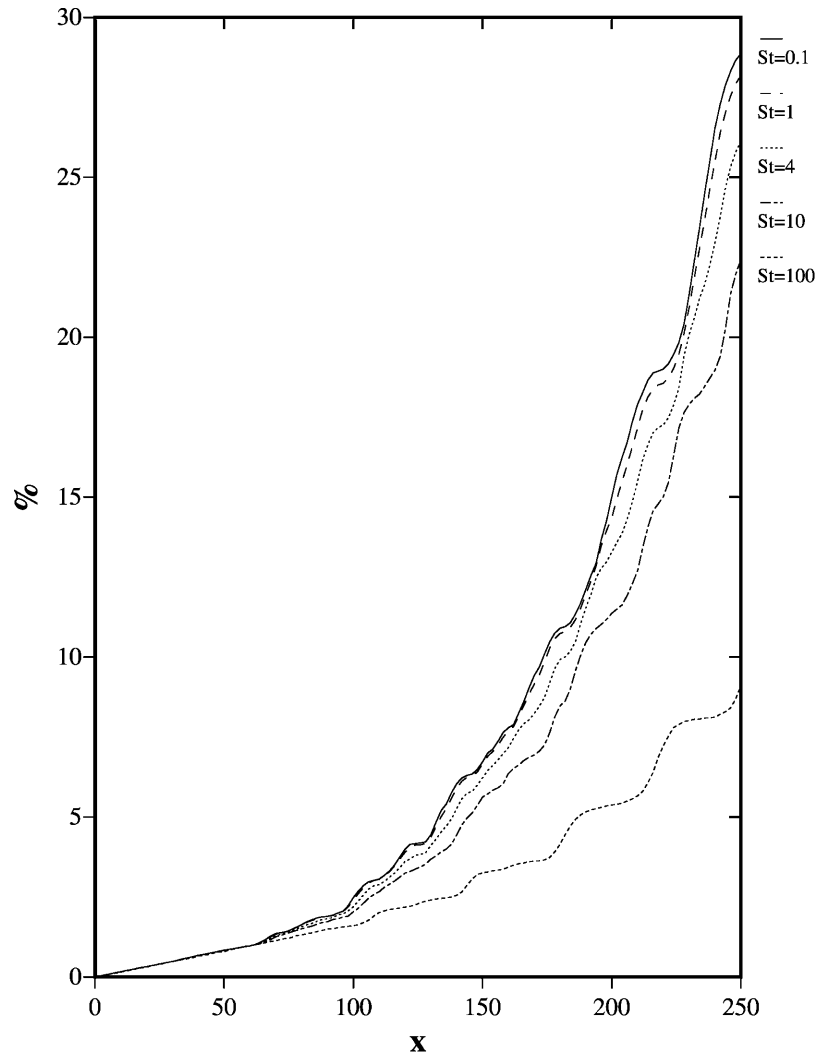


Figure 10. Effects of the Stokes number on the percentage of particles crossing streams.

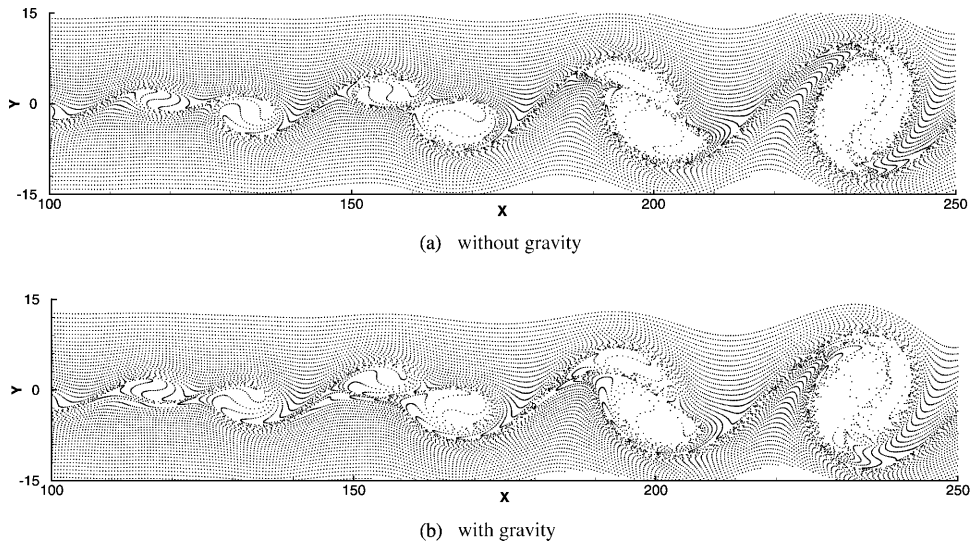


Figure 11. Effects of gravity on the particle dispersion pattern ($St = 4, t = 315$).

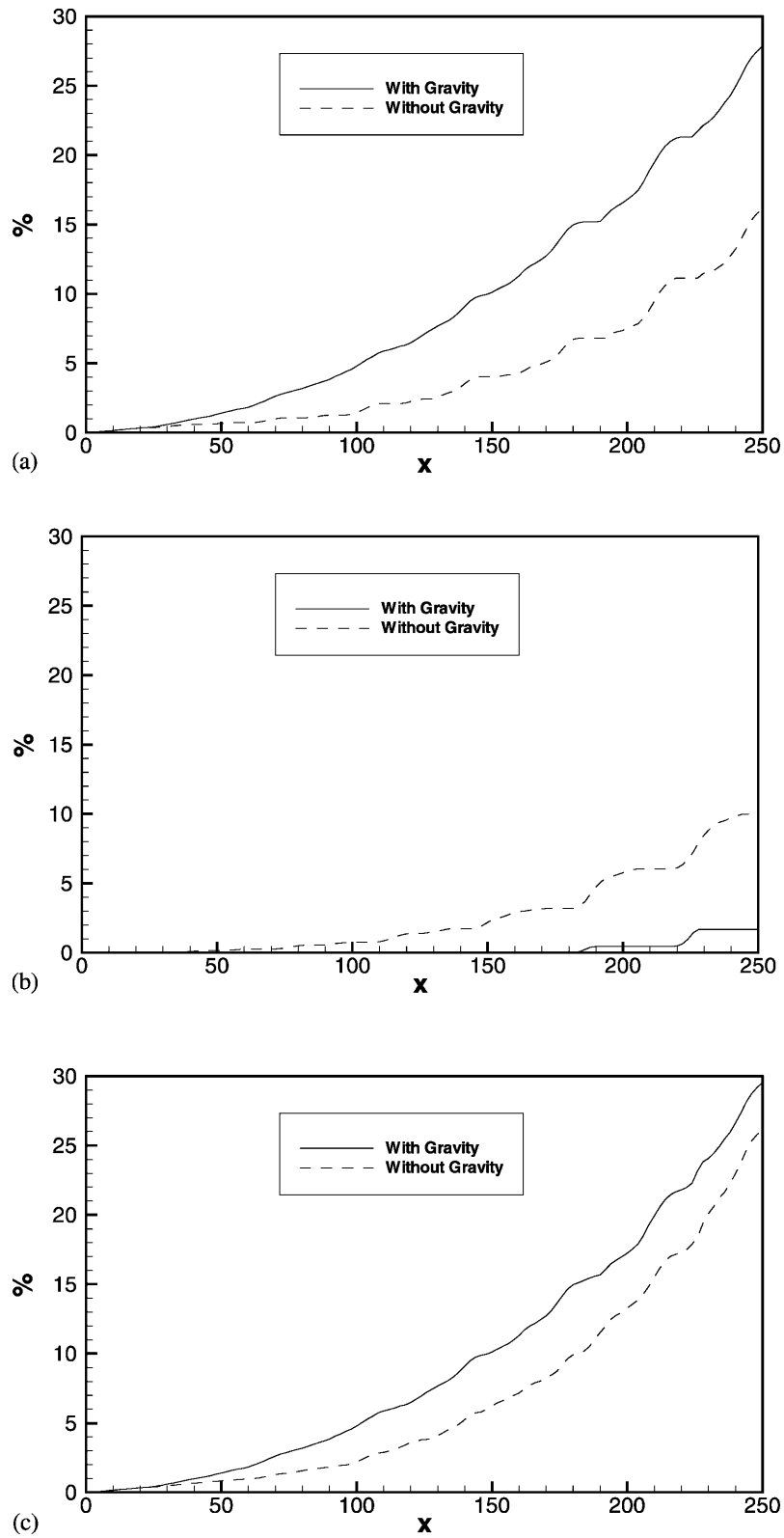


Figure 12. The effects of gravity on particles transported, $St = 4$. (a) Percentage of particles transported from upper stream to lower stream (b) Percentage of particles transported from lower stream to upper stream (c) Percentage of particles crossing stream.

of particles transported from one free stream to another is shown in Figure 12. Gravity is seen to enhance particle transport from the upper stream to the lower stream, but suppress the reverse process. The most interesting result is that the total percentage of particles transported across streams is increased with gravity. This is again related to the asymmetry in the present spatial mixing layer, discussed earlier. As the upper stream moves faster than the convection speed (U_c) of the large vortex structures while the lower stream moves slower than U_c , particles in the upper stream are influenced by faster rotating motions so that the upper stream brings more particles into the lower stream. Since gravity enhances particle transport in the more effective direction, the overall efficiency of particle transport is improved.

5. Discussions and Conclusion

Numerical simulation of particle dispersion has been carried out in a spatially developing mixing layer. The instantaneous particle distribution patterns and key statistical data have been analyzed. The study highlights the important effects of interacting vortex structures in nearby regions on particle transport, which are absent from the temporally developing mixing layers. Effects of the particle Stokes number have been carefully examined. The low, medium and high Stokes numbers lead to different instantaneous particle dispersion patterns in relation to the large vortex structures. Particle density concentration along the streamwise direction shows large variations, whose amplitudes increase with streamwise location. These reflect the different effects of vortex cores, braids and circumferences on particle dispersion, and the increasing strengths of the vortices along the streamwise direction. The dispersion pattern resulting from particles with randomly distributed sizes has also been analyzed. The mechanisms for particle dispersion in the spatial mixing layer have been further investigated by focusing on the particles that cross the streams. The number of particles moving from the upper stream into the lower is larger than that moving in the opposite direction. This is due to the asymmetric vortex structures developing from the spatial mixing layer. It is also related to the interactions between vortices in nearby regions, which are present only in the spatial mixing layer. The effects of gravity on particle transport and distribution have also been investigated. In addition to modifying the overall particle distribution, the presence of gravity increases the total percentage of particles being transported across streams. The above simulations have been limited to a transitional flow at low Reynolds and low Mach numbers, even though the methodology is designed for fully compressible flow. Previous studies by the authors and others have shown that free shear flows (e.g. mixing layers and jets) are dominated by two-dimensional large-scale structures, even at higher Reynolds numbers. So the above two-dimensional simulations are suitable and the conclusions about particle dispersion are valid until the Mach number is much larger. As the Mach number increases to 0.4 or larger, three-dimensional effects become important (Luo and Sandham, 1994). The effects of small-scale motions will also become more important, especially if higher Reynolds numbers are also used. The longer term goal of the study is to include high Mach number and high Reynolds number effects, although the computational cost is expected to be extremely high for spatial mixing layer simulations. The above results can also be made more general if the particle–particle interaction and/or the particle–fluid interaction are included. The Stokes number effects, for example, cannot be separated from the particle–particle collisions, if the particle sizes are sufficiently large. Therefore, the present study represents just one step towards solving the highly complex problem of particle dispersion under more realistic conditions.

Acknowledgments

The authors thank the Education Commission of the Chinese government for providing the first author with a one-year Overseas Scholarship to work in the Department of Engineering, Queen Mary College, University of London. Helpful discussions with Prof. N.D. Sandham of Southampton University are highly appreciated. The authors also thank Dr. X. Jiang and Mr. P. Humbert for their useful and informative discussions.

References

- Elghobashi, S., and Truesdell, G.C. (1992). Direct simulation of particle dispersion in a decaying isotropic turbulence. *J. Fluid Mech.*, **242**, 655–700.
- Elghobashi, S., and Truesdell, G.C. (1993). On the two-way interaction between homogeneous turbulence and dispersed solid particles. I: Turbulence modification. *Phys. Fluids A*, **5**, 1790–1801.
- Ho, C.M., and Huerre, P. (1984). Perturbed free shear layers. *Ann. Rev. Fluid Mech.*, **16**, 365–424.
- Inoue, O. (1995). Note on multiple-frequency forcing on mixing layers. *Fluid Dynam. Res.*, **16**, 161–172.
- Lele, S.K. (1992). Compact finite difference schemes with spectral-like resolution. *J. Comput. Phys.*, **103**, 16–42.
- Ling, W., Chung, J.N., Troutt, T.R., and Crowe, C.T. (1998). Direct numerical simulation of a three-dimensional temporal mixing layer with particle dispersion. *J. Fluid Mech.*, **358**, 61–85.
- Luo, K.H. and Sandham, N.D. (1994). On the formation of small scales in a compressible mixing layer. In *Fluid Mechanics and its Applications: Direct and Large-Eddy Simulation I* (P.R. Voke, L. Kleiser and J.-P. Chollet, eds.), pp. 335–346. Kluwer Academic, Dordrecht.
- Marcu, B., and Meiburg, E. (1996). The effect of streamwise braid vortices on the particle dispersion in a plane mixing layer. I. Equilibrium points and their stability. *Phys. Fluids*, **8**, 715–733.
- Marcu, B., Meiburg, E. and Raju, N. (1996). The effect of streamwise braid vortices on the particle dispersion in a plane mixing layer. II. Nonlinear particle dynamics. *Phys. Fluids*, **8**, 734–753.
- Martin, J.E., and Meiburg, E. (1994). The accumulation and dispersion of heavy particles in forced two-dimensional mixing layers, I. The fundamental and subharmonic cases. *Phys. Fluids*, **6**, 1116–1132.
- Maxey, M.R., and Riley, J.J. (1983). Equation of motion for a small rigid sphere in a nonuniform flow. *Phys. Fluids*, **26**, 883–889.
- Moin, P., and Mahesh, K. (1998). Direct numerical simulation: a tool in turbulence research. *Annu. Rev. Fluid Mech.*, **30**, 539–578.
- Moser, R.D., and Rogers, M.M. (1993). The three-dimensional evolution of a plane mixing layer: pairing and transition to turbulence. *J. Fluid Mech.*, **247**, 275–320.
- Poinsot, T.J., and Lele, S.K. (1992). Boundary-conditions for direct simulations of compressible viscous flows. *J. Comput. Phys.*, **101**, 104–129.
- Ramaprian, B.R., Sandham, N.D., Mungal, M.G., and Reynolds, W.C. (1989). Passive scalar for the study of the coherent structures in the plane mixing layer. *Phys. Fluids A*, **1**, 2034–2041.
- Rogers, M.M., and Moser, R.D. (1992). The three-dimensional evolution of a plane mixing layer: the Kelvin–Helmholtz rollup. *J. Fluid Mech.*, **243**, 183–226.
- Sandham, N.D., and Reynolds, W.C. (1989). Some inlet-plane effects on the numerically simulated spatially developing mixing layer. In *Turbulent Shear Flows*, Vol. 6, pp. 441–454. Springer-Verlag, New York.
- Snyder, W.H., and Lumley, J.L. (1971). Some measurements of particle velocity autocorrelation functions in a turbulent flow. *J. Fluid Mech.*, **48**, 41–71.
- Squires, K.D., and Eaton, J.K. (1994). Effect of selective modification of turbulence on two-equation models of particle-laden turbulent flows. *Trans. ASME, J. Fluid Eng.*, **116**, 778–784.
- Stanley, S., and Sarkar, S. (1997). Simulation of spatially developing two-dimensional shear layer and jets. *Theoret. Comput. Fluid Dynam.*, **9**, 121–147.
- Thompson, K.W. (1987). Time dependent boundary conditions for hyperbolic system. *J. Comput. Phys.*, **68**, 1–24.
- Truesdell, G.C., and Elghobashi, S. (1994). On the two-way interaction between homogeneous turbulence and dispersed solid particles. II: Particle dispersion. *Phys. Fluids*, **6**, 1405–1407.
- Vreman, A.W., Sandham N.D., and Luo, K.H. (1996). Compressible mixing layer growth rate and turbulence characteristics. *J. Fluid Mech.*, **320**, 235–258.
- Wang, L.P., and Maxey, M.R. (1993). Settling velocity and concentration distribution of heavy particles in homogeneous isotropic turbulence. *J. Fluid Mech.*, **256**, 27–68.
- Weisbrot, I., and Wygnanski, I. (1988). On coherent structure in a highly excited mixing layer. *J. Fluid Mech.*, **195**, 137–159.
- White, F.M. (1974). *Viscous fluid flow*. McGraw-Hill, New York.
- Wygnanski, I., and Weisbrot, I. (1988). On the pairing process in an excited plan turbulent mixing layer. *J. Fluid Mech.*, **195**, 161–173.